Dynamics of Carbon Monoxide Binding with Neuronal Nitric Oxide Synthase

Catherine Tetreau,*,‡ Martine Tourbez,‡ Antonius Gorren,§ Bernd Mayer,§ and Daniel Lavalette*,‡

Institut Curie, INSERM U350, Batiment 112, Centre Universitaire, 91405 Orsay, France, and Institut für Pharmakologie und Toxikologie, Karl-Franzens-Universität, 8010 Graz, Austria

Received January 19, 1999; Revised Manuscript Received March 23, 1999

ABSTRACT: The dynamics of CO rebinding with neuronal NO synthase (nNOS) following laser flash photolysis have been investigated from 293 to 77 K in the absence and presence of its substrate L-arginine. The distribution functions of the rate parameters $P(k)$ and of the activation enthalpy $P(H)$ were determined using the maximum entropy method. In a fluid solvent near room temperature, bimolecular rebinding is biphasic, as previously reported by several groups. However, measurement of the rotational correlation time shows that the apparent biphasic rebinding is not relevant to the genuine dynamics of NOS. In addition to native dimeric nNOS, another species (possibly aggregated or partially unfolded conformation) with different hydrodynamic characteristics is responsible for the faster rebinding process. In a rigid environment at low temperature, the geminate internal rebinding is not affected by the presence of the nonnative species. nNOS exhibits a bimodal distribution of CO activation enthalpy with $P(H)$ consisting of two distinct bands with temperature-dependent amplitudes down to 77 K. The similarity of these findings with those recently reported for cytochromes P-450 suggests a common hierarchical organization of conformational substates, with a splitting of each conformational substate into a doublet. Thus, thiolate-coordinated heme proteins are in clear contrast to histidine-coordinated oxygen-transport heme proteins. The present results with nNOS provide additional support to previous arguments incriminating the thiolate ligand as responsible for the splitting of conformational substates.

Proteins can assume a very large number of nearly isoenergetic conformational substates (CS)[1] differing slightly in structure as well as in reactivity. In particular, ligand binding occurs with a different activation enthalpy and rate. The thermodynamics and the kinetics of a protein ensemble must be described by probability distributions $P(H)$ and $P(k)$ of the activation enthalpy H and of the reaction rate parameter k, respectively (*1*).

The rate distribution manifests itself as nonexponential reaction kinetics, such as observed in laser flash photolysis studies of different classes of CO, O_2, and NO binding proteins (*1*−*5*), under conditions where fluctuations between substates are suppressed as in a rigid environment below the glass transition temperature of the solvent (T_g). Exponential kinetics, such as usually observed in a fluid environment at room temperature, are a consequence of fast equilibrium fluctuations between CS which cause the $P(k)$ distribution to collapse into a unique average value.

The energy landscape of carboxymyoglobin has been most extensively investigated and has been for many years a paradigm for the hierarchical organization of protein CS into a number of tiers, CS^0, CS^1, CS^2, etc., characterized by different heights of the free energy barriers separating individual CS (*6*−*8*). However, more work is required to determine which characteristics of the energy landscape of proteins are general, which are specific, and which are functionally relevant.

Thus, we recently found that the hierarchy of CS of cytochromes P-450 is more complex still than that of oxygen-binding hemoproteins (*4*). In cytochromes P-450, CS appear in pairs, or "doublets", with different dynamic properties. The consequence is that $P(H)$ is bimodal, consisting of two temperature-independent distributions but combined in a proportion which, even below T_g, keeps changing with temperature.

Cytochromes P-450 are heme−protein monooxygenases sharing a common active site consisting of a thiolate-coordinated iron protoporphyrin IX. They perform a great diversity of biological functions and are often characterized by a high substrate specificity. Despite this diversity, P-450$_{cam}$, P-450$_{LM2}$, and P-450$_{scc}$ display a common hierarchical organization of their CS. The structural fluctuations responsible for the CS splitting are not identified yet, though several arguments suggest that the proximal thiolate ligand might be involved.

We now report on nitric oxide synthase (NOS; for recent reviews, see refs *9*, *10*), which is closely related to cytochromes P-450 since the active center of the NOS oxygenase domain also consists of a thiolate-coordinated heme. NOS catalyzes an NADPH- and O_2-dependent five-electron oxidation of L-arginine to generate L- citrulline and NO, which is a key mediator in neural transmission, cytoprotection, and cardiovascular functions.

* To whom correspondence should be addressed. Phone: 33-1-69 86 31 81. Fax: 33-1-69 07 53 27. E-mail: Daniel.Lavalette@curie.u-psud.fr. E-mail: Catherine.Tetreau@curie.u-psud.fr.

‡ Centre Universitaire.

§ Karl-Franzens-Universität.

[1] Abbreviations: myoglobin, Mb; hemoglobin, Hb; hemerythrin, Hr; azurin, Az; conformational substates, CS; maximum entropy method, MEM; neuronal nitric oxide synthase, nNOS; nicotinamide adenine dinucleotide phosphate, NADPH; flavin adenine dinucleotide, FAD; flavin mononucleotide, FMN; L-arginine, L-Arg; (6*R*)-tetrahydrobiopterin, BH4; ethylene glycol, EG; tris(hydroxymethyl)aminomethane, Tris; ethylene glycol bis(β-aminoethyl ether) *N*,*N*,*N*′,*N*′-tetraacetic acid, EGTA.

10.1021/bi9901026 CCC: $18.00
Published on Web 05/14/1999

The three different isoforms of NOS are either constitutive (neuronal, nNOS, and endothelial, eNOS) or inducible (iNOS). All NOS isoforms are homodimers, with each subunit composed of two functional domains. The carboxy-terminal reductase domain contains binding sites for NADPH, FAD, FMN, and calmodulin. The amino-terminal moiety is an oxygenase domain that binds iron protoporphyrin IX, L-arginine, and a cofactor (6*R*)-tetrahydrobiopterin (BH4). NOS is active as a dimer and requires BH4 for full activity. The crystal structures of a monomeric fragment (*11*) and of the fully functional iNOS oxygenase domain (*12*) have been recently reported.

In the present work, the kinetics of CO rebinding with nNOS have been investigated from 293 to 77 K. At room temperature, biphasic bimolecular CO rebinding is found to originate from protein species with widely different rotational correlation time. At low temperature the distribution functions $P(k)$ and $P(H)$ of the internal geminate rebinding reaction were determined using the maximum entropy method (MEM). The kinetics were independent of the proportion of the nNOS species responsible for the biphasic bimolecular rebinding. It turns out that the hierarchical organization of CS in NOS is similar to that found with cytochromes P-450, with two different populations of substates still equilibrating below T_g. This provides a new argument supporting the idea that the nature of the proximal iron ligand might determine the CS splitting observed in proteins related to P-450 cytochromes.

MATERIALS AND METHODS

Materials. Recombinant rat brain nNOS was purified from *baculovirus*-infected cells as described previously (*13*). The holoenzyme contained 0.5 BH4 molecule per oxygenase domain. The required amount of nNOS was diluted with ethylene glycol (EG) and buffer to reach the final working concentrations of 5 mg/mL NOS, 30 mM in Tris/HCl, 150 mM in NaCl, 1 mM in EGTA, 10 mM in mercaptoethanol, 250 μM BH4, and 60% (w/w) EG at pH 7.6. With 250 μM BH4 each oxygenase domain contained one effector molecule. In some experiments arginine was added at a concentration of 5 mM. The solubility of CO in 60% ethylene glycol is $\approx$1 mM. The ferrous CO complexes were prepared by passing a stream of CO above the protein solution submitted to gentle stirring at either 293 or 278 K and by adding a few microliters of a concentrated deaerated dithionite solution. CO binding was controlled by following the UV−vis absorption change of the solution. Complete reduction was achieved within 20−30 min. The amount of P-420 was estimated from the relative absorbances at 420 and 446 nm, using the extinction coefficients determined for the P-420 and P-450 forms of cytochrome P-450$_{cam}$, since the corresponding values for the P-420 form of NOS remain unknown.

Methods. The methods used to collect and process the data and to recover the rate parameter and enthalpy distributions have been described in detail in a previous work (*4*) and will only be briefly summarized here.

1. Data Collection. Carbonylated nNOS solutions in gastight square cuvettes were inserted in a liquid nitrogen cryostat (Oxford Instruments DN704). The sample was cooled below T_g in about 20 min. Systematic records were performed by cooling the sample in steps of 10 K at a rate of 1 K/min and allowing 15 min of equilibration once the desired temperature was attained. Photodissociation was achieved by the 10-ns pulse of the second harmonic (532 nm) of a Q-switched Nd:YAG laser (Quantel, France). Transient absorption changes, monitored at the peak of the Soret band (444 nm), were recorded over 2 decades in amplitude and 6−7 decades in time using a fast kinetic spectrometer setup.

2. Distribution of Rate Parameters Using MEM. At low temperature the kinetics, expressed by the survival fraction $N(t)$ of unrecombined molecules, are given by the weighted infinite sum of exponentials (1):

$$N(t) = \int_0^\infty P(k)\, e^{-kt}\, dk \qquad (1)$$

We used MEM to invert the Laplace transform (1) to get $P(k)$ from the observed kinetics $N(t)$ (*2*,*14*−*18*). The software based on the Cambridge algorithm and on the Memsys5 package (Maximum Entropy Data Consultants Ltd., Cambridge) works on a set of logarithmically spaced k values. Accordingly, absorbance changes and noise statistics were first converted to a logarithmic time base using a "logarithmic smoothing" subroutine. Since noise estimation is very critical in the MEM analysis (*2*), we regarded as real structures only those features which clearly persisted even after arbitrarily doubling the noise.

3. Computing the Enthalpy Distribution P(H). The basic assumption is that below the solvent's glass transition temperature T_g, all kinetics should be derived from one unique probability distribution of activation enthalpy $P(H,T_g)$ (*1*). The rate parameter k and the activation enthalpy H are connected by:

$$H = RT \ln A - RT \ln k \qquad (2)$$

giving, for the corresponding probability distributions,

$$P(H,T)\, dH = P(-RT \ln k)\, d(-RT \ln k)$$
$$P(H,T)\, dH = P(h)\, dh \qquad (3)$$

in which the variable $h = RT \ln k$ has the dimensions of an enthalpy. Since MEM directly outputs $P(\log k)$, a simple change of coordinates followed by renormalization yields the $P(H,T_g)$ profile. To determine its absolute position on the H scale, the preexponential factor A was obtained from the linear plot of the barycenter of a series of $P(h)$ at different temperatures (*4*).

4. Rotational Brownian Motion and Correlation Time Measurements. The rotational correlation times were determined using the transient optical absorption anisotropy method. The anisotropy (R) was induced by photodissociation of the CO−Fe(II) nNOS complex using a vertically polarized laser pulse. The anisotropy decay, $R(t)$, was recorded using a dual-beam device as described earlier (*19*). The correlation time ϕ was obtained by an exponential fit to:

$$R(t) = [A_v(t) - A_h(t)]/[A_v(t) + 2A_h(t)] = R_0 \exp(-t/\phi) \qquad (4)$$

in which A_v and A_h are the transient changes in absorbance measured with a polarization direction respectively parallel (vertical) and perpendicular (horizontal) to that of the photodissociating beam.

For a spherical particle, the Brownian rotational correlation time ϕ is given by the Stokes−Einstein equation:

$$\phi = \eta V/kT \quad (5)$$

in which η is the solvent's viscosity and V is the hydrated volume of the protein. Measurements were performed at a constant viscosity of 6 cP, either in 60% EG at 293 K or in 29% sucrose at 278 K. Viscosities were measured using Ubbelohde viscosimeters.

RESULTS

1. Fluid Environment at Room Temperature

At 278−293 K in a fluid solvent, conformational fluctuations are much faster than rebinding. The kinetics are therefore expected to consist of discrete exponentials and $P(k)$ of more or less narrow bands depending on the noise statistics. Under conditions of fast fluctuations, carbonylated nNOS follows the same global kinetic scheme as other proteins which bind a photolabile ligand (Scheme 1):

Scheme 1

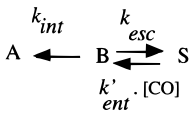

A denotes the state in which CO is bound to the heme. In state B the heme−CO bond has been photodissociated but the ligand remains within the protein. In S the ligand has left the protein and may exchange freely with other ligand molecules in the solvent.

1.1. Arginine-Free NOS. The kinetics and rate distribution of CO rebinding with arginine-free nNOS at 278 K in 60% EG are displayed in Figure 1. Numerical values are listed in Table 1. Three well-characterized rebinding processes can be distinguished.

The initial, faster phase, observed in the time range of 10 ns−1 μs, was independent of CO concentration. It corresponds to the geminate process, i.e., to CO molecules which recombine with a rate $k_{gem} = k_{int} + k_{esc}$, without leaving the protein. This process appears as one unique band G in the high (6−8 log k units) region of the rate distribution function.

The rates of the subsequent, slower processes, observed in the time range of 100 μs−100 ms, varied linearly with the CO concentration. This characterizes bimolecular rebinding processes after diffusion of CO out into the solvent with a global second-order rate k'_{on}. Two bands (bands I and II) located in the low (0−4 log k units) rate region of $P(k)$ reflect the biphasic character of the bimolecular rebinding process which is also clearly apparent in the decay shown in Figure 1a. The proportion $N_{esc} = k_{esc}/k_{gem}$ of molecules rebinding via the bimolecular processes was estimated to 0.64 from the relative area of the $P(k)$ bands.

1.1.1. Influence of Solvent and Temperature on the Bimolecular Rebinding Process at 278−293 K. Figure 2 shows a magnification of the bimolecular rebinding consisting of two peaks centered at log $k \approx 1.3 \pm 0.1$ (band I) and at log $k \approx 3.2 \pm 0.2$ (band II). For an easier comparison, the curves were renormalized to a total unit area. Rebinding experiments were performed in pure buffer (Figure 2a) and in 60% EG (Figure 2b) using NOS samples which were

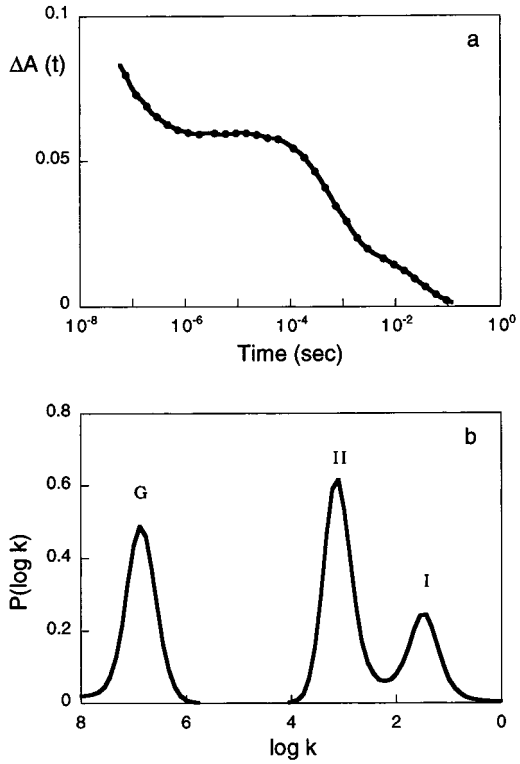

FIGURE 1: (a) Kinetics of CO rebinding with arginine-free nNOS (1 BH4/heme) measured at the peak of the Soret band (444 nm) in 60% EG at 278 K. (b) Normalized $P(k)$ rate distribution. Since our measurements begin at $t \approx 7\ 10^{-8}$ s, band G is not well-defined for rates $\geq 10^7\ s^{-1}$. The MEM calculations were performed by leaving the norm free, so that no arbitrary normalization of the kinetics was required.

prepared, reduced, and photolyzed at 293 K (dotted lines) or 278 K (full lines). Some variations in band positions are not surprising owing to the different solvent, temperature, and possibly CO solubilities, as well as to different amounts of band overlap. They are however of secondary importance. The most salient finding is that the relative proportion of both bands critically depends on the nature of the solvent and on the temperature at which NOS was reduced. Even in 60% EG, the ratio between bands I and II fluctuated from one sample to another, suggesting some instability in native NOS preparations. The eventuality that P-420 formation could spoiled the kinetics could be ruled out. The amount of P-420, estimated from the UV−vis absorption spectrum, was currently 8−10%, thus leading to a contribution of less than 3% to the kinetics recorded at 444 nm. A typical spectrum is given in Figure 3. We suspect protein conformational or oligomeric heterogeneity. To test this hypothesis, we attempted to estimate the size of the protein species responsible for bands I and II by measuring their Brownian rotational correlation time.

1.1.2. Brownian Rotational Correlation Time in the Bimolecular Rebinding Bands I and II. Ideally, measurements of the Brownian rotational correlation time should be performed in conditions under which either band I or II largely predominates, i.e., by preparing the CO−Fe(II) nNOS complex in aqueous buffer at 278 K (log $k = 1.2$; Figure 2a, full line) and in EG at 293 K (log $k = 3.2$; Figure 2b, dotted line). The viscosity of 60% EG at 293 K is equal to 6 cP. The correlation time in pure buffer was however too short to be measured accurately with the dual-beam polariza-

Table 1: CO Rebinding with nNOS at 278 K in 60% EG[a]

	geminate phase[b]		bimolecular phase[c]		
	k_{gem} (10^6 s^{-1})	N_{esc}	$k'_{on,II}$ (10^6 M^{-1} s^{-1})	$k'_{on,I}$ (10^4 M^{-1} s^{-1})	% species I
Arg-free nNOS	8.0	≤0.64	1.3	2.8	31
Arg-bound nNOS	4.6	≤0.87	1.0	2.2	69

[a] The rate parameters correspond to the peak values of the distributions. The relative contributions were calculated from the relative band areas. Bimolecular rate parameters were calculated assuming [CO] ≈ 1 mM. [b] Given the laser time resolution, part of the geminate process escaped detection. Due to these instrumental limitations, error bars on the geminate rate constants cannot be evaluated, and N_{esc} is strictly a higher limit to the true escape yield. [c] Errors on the bimolecular rate constants and on the proportion of species I are about 10%.

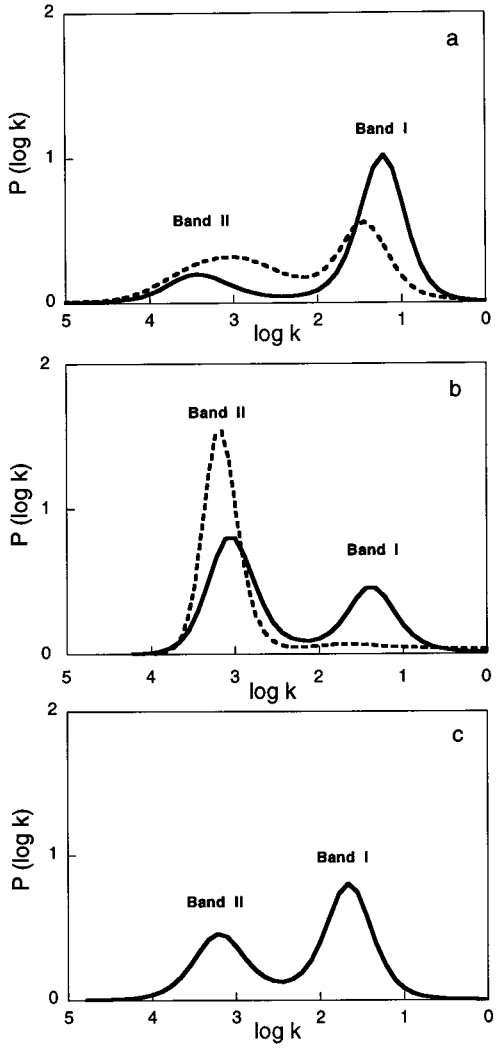

FIGURE 2: Normalized $P(k)$ distributions for the bimolecular rebinding process of CO with arginine-free nNOS (a) in aqueous buffer, (b) in 60% EG, and (c) in 29% sucrose, at 293 K (dotted lines) and 278 K (full lines).

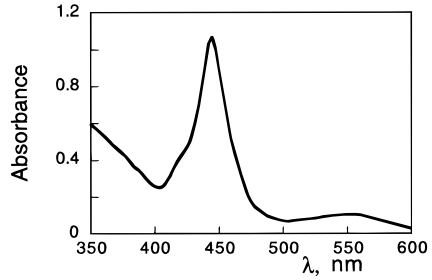

FIGURE 3: Absorption spectrum of the reduced form of arginine-free NOS (15 μM) in the presence of 1 atm of CO, measured in a 4-mm optical cell (278 K, Tris buffer). The change between the beginning and end of the kinetic measurements at $T \leq 278$ K was always negligible.

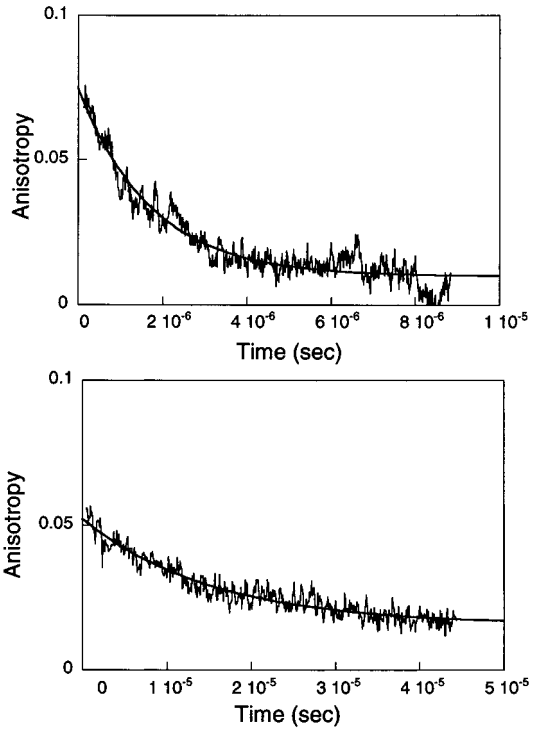

FIGURE 4: Anisotropy decay of the transient bimolecular rebinding of CO with nNOS. In sucrose/water (top) rebinding was predominantly from band I, whereas in 60% EG (bottom) rebinding was almost exclusively from band II (see Figure 2). The lines are single-exponential fits. The nominal viscosity was 6 cP in both experiments. Note the 5-fold change in time scale.

tion setup. The viscosity of the buffer solution was then adjusted also to 6 cP by adding 29% sucrose whose size is large enough to minimize solvent−protein interactions. In sucrose, the rebinding kinetics were not significantly modified, but the ratio band I/band II was unfortunately somewhat less favorable than in pure buffer (Figure 2c).

The relatively small initial anisotropy is due to the unfavorable laser excitation wavelength. Its decay was however quite measurable (Figure 4). Single-exponential fits yielded a correlation time $\phi = 1.7 \pm 0.1$ and 15.3 ± 3.0 μs for band I (sucrose, Figure 4, top) and band II (EG, Figure 4, bottom) at 6 cP, respectively. According to eq 5**,** this indicates that the nNOS species rebinding via band II has a hydrated volume about 10-fold that of the species rebinding via band I. The hydrodynamic radii of the equivalent sphere are 66 Å (band I) and 142 Å (band II).

1.2. Arginine-Bound NOS. MEM analysis of CO rebinding with nNOS in the presence of arginine is displayed in Figure 5.

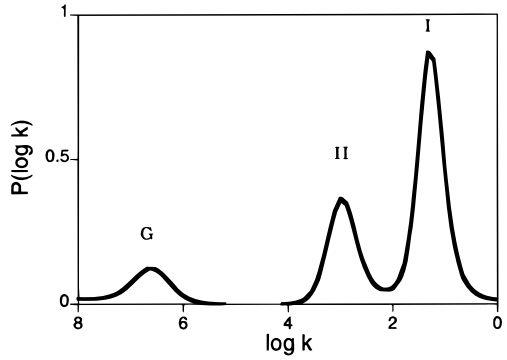

FIGURE 5: $P(k)$ distribution for the global kinetics of CO rebinding with nNOS in the presence of 5 mM arginine measured at the peak of the Soret band (444 nm) in 60% EG at 278 K (compare with Figure 1b).

Compared to the substrate-free form (Figure 1), the global yield of the bimolecular phase is increased from 0.64 to 0.87. Bimolecular rebinding is also biphasic, but the absence of shift in the band position indicates that the bimolecular rebinding rates are unaffected by arginine. Comparison with Figure 1 shows that band I now dominates bimolecular rebinding.

2. Rigid Environment and Low Temperature

In contrast to cytochrome P-450, we observed a reversible precipitation of nNOS below 200 K in glycerol/water, where most low-temperature experiments are usually performed. The geminate kinetics were therefore measured in 60% EG in the temperature range 77−140 K, i.e., below the glass transition temperature ($T_g \approx 140$ K).

As usual, the amplitude of the bimolecular process progressively decreased upon decreasing the temperature and vanished at about 200 K. Below 200 K the high viscosity of the medium prevented CO escape from the protein and only the geminate process from within the protein subsisted ($k_{gem} = k_{int}$). The geminate process became increasingly slower.

Because of the presence of the two nNOS species contributing to the bimolecular rebinding (see above) and because cytochrome P-450 geminate rate distributions are known to be intrinsically bimodal at low temperature (*4*), we were dreading observing a rather intricate kinetic pattern. We therefore varied the initial amount of species II from 62% to 100% by changing the temperature of preparation of the nNOS (see Figure 2). No significant changes in the low-temperature geminate kinetics and enthalpy distributions could be observed upon varying the amount of species II. This indicates that internal rebinding, being a heme-localized process, is insensitive to the circumstances giving rise to the nNOS species heterogeneity, whatever the latter may be.

The kinetics were nonexponential and covered several time decades. The rate distributions of the geminate CO rebinding with arginine-free and arginine-bound NOS at three selected temperatures are shown in Figure 6. According to eq 3, the profile $P(h,T)$ mirrors that of $P(H)$. Below T_g in the absence of protein conformational fluctuations, $P(H)$ should remain invariant and equal to $P(H,T_g)$. However, a spectacular change of shape with temperature is clearly visible in Figure 6 indicating that $P(h)$ cannot be attributed to a unique bimodal $P(H)$ distribution but rather to a superposition of (at least) two independent enthalpy subdistributions. A

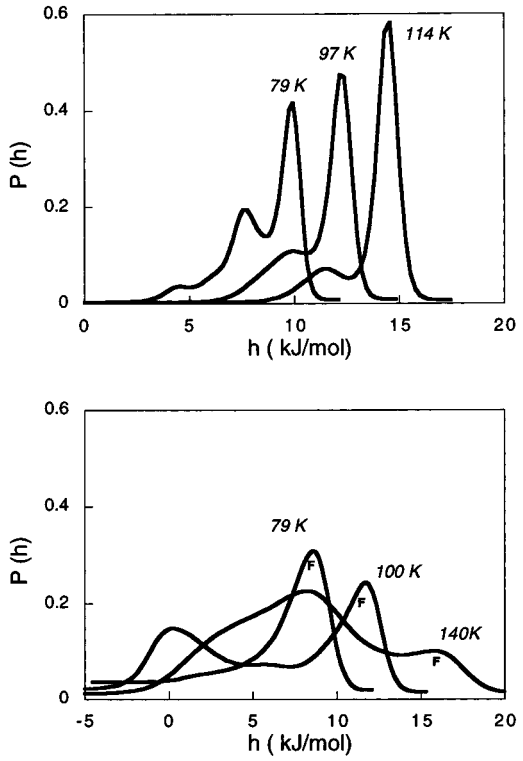

FIGURE 6: $P(h) = P(RT \ln k)$ for the geminate kinetics of the arginine-free (top) and arginine-bound (bottom) forms of nNOS in 60% EG. The shoulder near 5 kJ/mol in the 140 K distribution of arginine-bound nNOS is not regarded as a significant structure, since its amplitude varied with sample and noise statistics.

similar observation has been already reported for cytochromes P-450 (*4*). Since the present data are insufficient to warrant more than two bands, we develop the enthalpy distribution according to:

$$P(H,T) = \alpha_{fast}(T)P_{fast}(H) + \alpha_{slow}(T)P_{slow}(H) \qquad (6)$$

in which α_{fast} and α_{slow} are temperature-dependent weighting factors of the two subpopulations. A Gaussian decomposition yielded $P(H,T_g)_{fast}$ and $P(H,T_g)_{slow}$ which were independently normalized. The final normalized and temperature-invariant $P(H,T_g)$ are given in Figure 7.

For the substrate-free protein, the variation in the shape of $P(h)$ upon decreasing the temperature (Figure 6, top) clearly indicates that the amplitude of the population corresponding to "fast" rates decreases, while that of "slow" rates increases upon lowering the temperature. The opposite trend is found in the presence of arginine (Figure 6, bottom).

A rough estimation of the thermodynamic parameters of the ratio "$\alpha_{fast}/\alpha_{slow}$" yields: $\Delta S_0/R = 0.9(\pm 0.8)$ and $\Delta H_0 = 1.3(\pm 0.6)$ kJ·mol^{-1} for arginine-free NOS and $\Delta S_0/R = -6(\pm 0.4)$ and $\Delta H_0 = -5.1(\pm 0.4)$ kJ·mol^{-1} for arginine-bound NOS. These values are of a similar order of magnitude as those determined for cytochromes P-450 (*4*).

Except for the "slow" population of the arginine-bound form (dotted band of Figure 7, bottom), enthalpy distributions peak at very low values. The physically unreasonable negative values are indicating that the two-Gaussians model is only an approximation.

DISCUSSION

Geminate recombinations locally probe the reactivity of the active site with the ligand already present in the heme

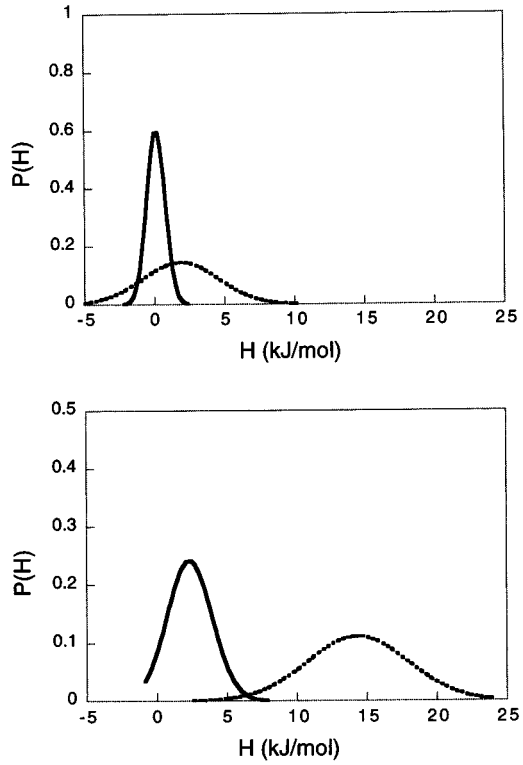

FIGURE 7: Normalized enthalpy subdistributions $P(H,T_g)$ for CO geminate rebinding with arginine-free (top) and arginine-bound (bottom) nNOS forms. Full and dotted lines correspond to the enthalpy distributions of the "fast" and "slow" sets of substates, respectively.

pocket. At room temperature, their rate often competes with ligand escape from the protein and with the time resolution of the equipment. It is generally difficult to exclude experimental distortions. Geminate recombinations are therefore best investigated in a rigid environment at low temperature.

In bimolecular rebinding, the intrinsic reactivity of the heme is modulated by the dynamic characteristics of the protein matrix permitting ligand entry to the heme pocket. Therefore bimolecular processes and geminate recombinations reflect different but complementary aspects of ligand binding to a heme protein. The former may be sensitive to quaternary structural changes and thus pertains to the particular protein being investigated. The latter, being more local, is useful for comparing different proteins which share a common active center. In this discussion we address two main issues: (i) how can the complicated bimolecular rebinding of CO nNOS be reconciled with what is known about the quaternary structure of the protein and (ii) are these peculiarities affecting the geminate recombinations in nNOS and how do the latter compare with those of cytochromes P-450?

1. Fluid Environment at 293−278 K

1.1. Bimolecular Rebinding, nNOS Conformation, and Oligomeric State. Biphasic bimolecular rebinding of CO with nNOS was first observed by Matsuoka (*20*). Scheele et al. (*21*) reported that three or four exponentials were required to fit CO bimolecular rebinding with nNOS and that the exponentials tend to group into two distinct time regimes with rates centered at values quite consistent with those measured in this work, given the different experimental conditions. To interpret their observations, the authors postulated a quasi continuous and bimodal distribution of conformations clustering about the two most common forms. Resonance Raman studies revealed the presence of dual Fe−CO and C−O stretch band frequencies of the nNOS−CO complexes (*22*). Relying on the available kinetic data (*20*, *21*), the authors suggested that arginine-free nNOS presents two conformations, closed and open (called α and *β*), in roughly similar proportions, whereas only one (α conformation) was present in the presence of arginine. The occupation of the distal pocket by BH4 or water was invoked to explain the presence of the α conformation in the substrate-free protein.

Though our finding that $P(k)$ consists of two bands clearly supports the work of Scheele et al., our measurement of the rotational correlation time provides additional information. The two bimolecular rates correspond to rebinding with protein species having very different hydrodynamic properties.

A detailed discussion of the anisotropy decays would involve additional knowledge about the real shape of the protein as well as about the orientation of the transition dipole moment μ of the heme relative to the protein axes. According to theory (*23*) a single-exponential anisotropy decay is obtained either for oblate ellipsoids irrespective of the orientation of μ or for prolate ellipsoids, if μ is approximately parallel to the symmetry axis of the ellipsoid; in either case, the apparent correlation time is an increasing multiple of that of a sphere of equal volume as the axial ratio of the ellipsoid increases. Two-exponential anisotropy is obtained with prolate ellipsoids in the situation where μ is approximately perpendicular to the symmetry axis: three-fourths of the anisotropy is decaying with the same ϕ value as the equivalent sphere and one-fourth with a considerably longer correlation time. For other orientations of μ, up to three exponentials may contribute to the anisotropy decay. Multiple-exponential anisotropy decays are in practice difficult to resolve, especially with "single shot" records such as performed in the present work. In addition, since the orientation of μ is not known for nNOS, only limiting cases can be considered.

We first estimate the correlation time expected for a 320-kDa native dimer by using an empirical relationship based on our past experience with rotational measurements of proteins over a wide range of molecular weights:

$$\phi = 2 \times 10^{-4} M^{1.11} \qquad (7)$$

where ϕ is the correlation time measured in nanoseconds at 1 cP and 20 °C and M is the molecular weight in daltons. Equation 7 works well for globular and moderately flattened or elongated proteins (Lavalette, unpublished results). At 6 cP and 278 K the expected correlation time of 1.6 μs compares very well with the experimental value of $\phi = 1.7$ μs found for the band I species. The assignment of band I species, which is by far dominant in aqueous buffer, to the native dimeric nNOS is in agreement with the molecular weight of nNOS, and the corresponding hydrodynamic radius $R_h = 66$ Å is also consistent with $R_h = 73$ Å determined for native dimeric nNOS using dynamic light scattering (*24*).

The anisotropy decay for band I species in 29% sucrose consists of a single-exponential plus a small residual, due to

Table 2: Preexponential Factors, Peak Enthalpies, and Enthalpy Widths Determined for the "Fast" and "Slow" Subpopulations below $T_g = 140$ K

	fast geminate phase			slow geminate phase		
	log A_{fast} (s^{-1})	H_{fast} (kJ/mol)	width[a] (kJ/mol)	log A_{slow} (s^{-1})	H_{slow} (kJ/mol)	width[a] (kJ/mol)
Arg-free nNOS	6.6 (0.2)	0.1 (0.2)	1.5 (0.2)	6.0 (0.2)	1.8 (0.2)	6.4 (0.2)
Arg-bound nNOS	7.2 (0.2)	2.3 (0.2)	3.8 (0.2)	8.0 (0.2)	14.3 (0.5)	8.4 (0.2)

[a] Full width at half-maximum of the enthalpy distribution. Values in parentheses are estimated standard deviations.

unavoidable contamination by the 10-fold longer correlation time of band II species (see Figures 2 and 3). The simple exponential decay and the correct prediction of ϕ by eq 7 imply that the protein deviates only moderately from a spherical shape. The axial ratio of about 20 deduced from molecular weight and diffusion coefficient (*24*) is certainly too high to be consistent with the present measurements. However, the estimation of axial ratios involves a precise knowledge of partial specific volume and protein hydration. A plausible explanation could be that the average values assumed to estimate the axial ratio significantly differ from the exact values of nNOS.

Band II species may then correspond to either an aggregated, a partially unfolded, or a misfolded protein conformation with a larger axial ratio. These views are consistent with the poor reproducibility of the amount of band II species from sample to sample as well as among authors, a fact which seems to render a simple conformational equilibrium rather unlikely. The hydrodynamic radius of the species rebinding via band II is about 142 Å, a result which is also in agreement with dynamic light scattering experiments where a minor component with $R = 170$ Å was detected and attributed to aggregation (*24*). The anisotropy plateau in Figure 4 would then be due to some amount of still larger aggregates.

The rate of CO bimolecular rebinding with band II species is increased by about 2 orders of magnitude compared to its value for the native protein (Table 1), indicating that the protein matrix of this species is sufficiently perturbed to allow an easier CO entry into the heme pocket compared to the native structure. The important conclusion to be drawn is that the apparent biphasic bimolecular rebinding is not relevant to the genuine dynamics of native nNOS which exclusively rebinds via band I.

1.2. Role of Arginine. In agreement with other studies (*20, 21, 25, 26*), we observed CO bimolecular rebinding to slow in the presence of arginine. The MEM analysis of the decays indicates however that the decrease of the bimolecular rate is only apparent. Indeed the mean rates of bands I and II are not affected, only their ratio is changed. Apparently arginine stabilizes the native structure. The absence of variation in the CO bimolecular rebinding rates upon substrate binding is quite consistent with the idea of a rather wide active site. The structure of the Fe(II)−CO complexes of NOS is unknown. However, the crystal structures of the Fe(III) forms of a monomeric fragment and of the fully functional iNOS oxygenase domain (bound or not with its substrate) have been recently determined by X-ray diffraction *(11, 12)*. The NOS distal pocket, primarily constructed from β-sheets, differs considerably from the distal pockets of cytochromes P-450 and oxygen carrier hemoproteins. The NOS distal pocket is highly flexible and open. In addition, in the arginine-bound form, the porphyrin ring is significantly bent and the arginine guanidinium group is stacked against pyrrole ring A *(12)*. The lateral displacement of the substrate away from the iron axis may perhaps account for the absence of steric interaction between CO and arginine. The lateral displacement of the substrate is also supported by a recent pulsed ENDOR spectroscopic study indicating that the guanidino nitrogen of arginine bound to nNOS is located at a relative short distance from the heme iron (about 4 Å) but is displaced from the heme normal by about 1−2 Å *(27)*.

The presence of a substrate within the heme pocket was found to interfere with ligand binding in the case of the highly substrate-selective cytochromes P-450_{cam} and P-450_{scc}. In contrast, P-450_{LM2} has a wide distal pocket which is able to accommodate a variety of large substrates that apparently do not interfere with CO binding (*4, 28, 29*).

1.3. Geminate Recombinations. In principle, each elementary rate constant of Scheme 1 can be calculated given k_{gem} and N_{esc}. However, due to experimental limitations, neither the amplitude nor the rate of the fast geminate phase can be determined accurately at room temperature. Given the laser time resolution, one cannot be sure that the fast phase seen at room temperature represents the whole geminate process and therefore that the measured escape yield is accurate enough. Table 1 shows that substrate binding does not affect much the apparent rate of the geminate phase. Extrapolation of the low-temperature data is rendered difficult because the individual $P(H)$ is expected to become intrinsically temperature-dependent above T_g. Data about this intermediate regime are not available yet, and a discussion of room-temperature geminate recombinations will require additional work.

2. Rigid Environment and Low Temperatures

2.1. Hierarchical Organization of CS. While in the extreme regime of fluid environment the rate of equilibrium fluctuations is much faster than that of rebinding, the opposite situation prevails in a rigid environment where fluctuations are frozen; at intermediate temperatures/viscosities, both processes may be on a comparable time scale, and analysis of the results becomes very difficult. Additional complexity can also result from nonequilibrium relaxation of the protein triggered by ligand dissociation *(16)*. In this work, we did not attempt to analyze the results in the intermediate range of temperatures, and we focused on a description of the CS at $T < T_g$ where the rate distribution simply reflects the histogram of the CS distribution.

The CO rebinding kinetics below 140 K are explained by the distributions of activation enthalpies shown in Figure 7, their temperature dependence, and the preexponential factors listed in Table 2. The most salient finding is that the enthalpy distribution $P(H)$ is a sum of two independent subdistributions, $P_{fast}(H)$ and $P_{slow}(H)$, with variable amplitudes down to 77 K.

Before discussing the properties of nNOS enthalpy distribution for geminate rebinding, it must be emphasized that the subdistributions, which we shall be discussing now, have nothing in common with the two species discussed previously in the context of bimolecular rebinding. The low temperature and the rigid environment cannot possibly permit a reequilibration between native and aggregated or unfolded states. Experimentally, no significant changes in the enthalpy distributions $P(H)$ could be observed upon varying the initial amount of band II from 62% to 100% by changing the temperature of preparation of the nNOS sample. This illustrates the localized nature of geminate rebinding and is rather in favor of the assignment of band II to aggregated species.

The behavior of nNOS at low temperature is quite similar to that found for cytochromes P-450. It differs markedly from that reported previously for other proteins (Mb, Hb, Hr, Az) for which only one single, temperature-invariant enthalpy band was observed below T_g.

In cytochromes P-450 as well as in NOS, the fact that each normalized subdistribution ($P_{fast}(H)$ or $P_{slow}(H)$) is temperature-independent below T_g implies that each represents one subset of CS and that the CS within one set ("fast" or "slow") are "frozen", i.e., thermodynamically disconnected. On the other hand, thermal equilibration between the subdistributions down to 77 K implies that each "fast" substate is connected with one "slow" substate and that both still slowly interconvert down to 77 K. As discussed previously (*4*), these two statements are not incompatible, provided that the height of the energy barrier connecting each couple of fast and slow substates is small, compared to that separating CS within each set. A free-energy diagram showing the possible connections of the various substates is given in Figure 8 of ref *4*. It explains how the subpopulations may thermally equilibrate during cooling, whereas higher barriers prevent the CS to interconvert during the much faster rebinding experiment.

Spectroscopic and kinetic studies of Mb (*6*, *7*) have revealed that CS can be described as a hierarchy of several tiers (CS^0, CS^1, CS^2, etc.) arranged by decreasing barrier heights. This model was adapted to account for the particular kinetic connections of cytochromes P-450 (*4*). CS^0 substates, which mainly differ by the Fe−C−O geometry/environment, are characterized by different infrared stretch bands of CO. Such states cannot be responsible for the bimodal enthalpy distributions since they do not equilibrate below T_g (*30*−*32)*. Evidence for CS^1 substates comes from the nonexponential rebinding kinetics at low temperature and from the resulting enthalpy spectrum. The particular observations with cytochromes P-450 and with NOS as well can be explained by assuming that each CS^1 substate is split into a doublet, with a "fast" and "slow" component. The presence of subdistributions even with substrate-free forms rules out the substrate as a cause of the existence of doublet substates. The structural perturbation connecting "fast" and "slow" reacting sets of substates must involve only small residual internal motions since most motions are suppressed in a rigid glass below T_g.

Although structural evidence is not yet available, we believe that the similarity of behavior of NOS and cytochromes P-450 provides additional support to our previous suggestion that the proximal residue of the heme might be at the origin of the splitting of CS. The most obvious local difference between Mb and Hb on the one hand and cytochromes P-450 and NOS on the other hand is the replacement of the bulky and rigid proximal histidine by a less compact and possibly more mobile thiolate ligand. In P-450 and NOS, the cysteine sulfur is located near the N-terminal end of a helix where it accepts hydrogen bonds from peptide NH groups attenuating its electrostatic charge (*29)*. Any residual motions of the thiolate would affect directly the amount of hydrogen bonding, which in turn would change the effective charge borne by the thiolate. CO rebinding rates are known to be highly sensitive to the charge of the proximal ligand (*33)*, so that two subpopulations differing only by subtle changes in the thiolate orientation may be characterized by quite different enthalpy distributions.

2.2. Substrate Binding. Peak activation enthalpies and bandwidths systematically smaller than corresponding values for myoglobin have been reported for cytochromes P-450. The two enthalpy peaks for the arginine-free form of nNOS (Figure 7, top, and Table 2) are smaller still than for $P\text{-}450_{LM2}$ and correspond to the smallest values ever reported. This is in good agreement with the idea of a wide active site supported by X-ray diffraction data mentionned above. Surprisingly, binding of arginine does not affect much the enthalpy of the fast subpopulation of CS but has a pronounced effect on the slow subpopulation. Moreover the relative amplitude of both subpopulations is reversed upon arginine binding. The reason for these differences is quite intriguing. Given the hypothesis that "slow" and "fast" subpopulations of CS differ by subtle changes in the proximal side structures, their different sensitivity to arginine binding could hardly be explained by invoking steric interactions of arginine with CO rebinding. In contrast, modulation of the CO rebinding rate by electrostatic interactions with arginine may be influenced by the proximal side structure.

SUMMARY OF CONCLUSIONS

Bimolecular rebinding of CO with nNOS near room temperature is distinctly biphasic. This heterogeneity is due to the coexistence of either an aggregated, a partially unfolded, or a misfolded conformation in addition to native dimeric nNOS.

At low temperature, the amount of these nonnative forms does not affect geminate rebinding. The enthalpy distribution consists of two distinct bands which are still in thermal equilibrium down to 77 K. nNOS thus behaves quite similarly to cytochromes P-450. This finding provides further support to the idea that the thiolate ligand might be at the origin of the particular hierarchical organization of conformational substates of this class of heme proteins compared to oxygen-transport proteins such as myoglobins and hemoglobins.

REFERENCES

1. Austin, R. H., Beeson, K. W., Eisenstein, L., Frauenfelder, H., and Gunsalus, I. C. (1975) *Biochemistry 14*, 5355−5373.
2. Lavalette, D., Tetreau, C., Brochon, J.-C., and Livesey, A. (1991) *Eur. J. Biochem. 196*, 591−598.
3. Ehrenstein, D., and Nienhaus, G. U. (1992) *Proc. Natl. Acad. Sci. U.S.A. 89*, 9681−9685.
4. Tétreau, C., Di Primo, C., Lange, R., Tourbez, H., and Lavalette, D. (1997) *Biochemistry 36*, 10262−10275.

5. Mitchell, D. M., Müller, J. D., Gennis, R. B., and Nienhaus, G. U. (1996) *Biochemistry 35*, 16782−16788.
6. Ansari, A., Berendzen, J., Bowne, S. F., Frauenfelder, H., Iben, I. E. T., Sauke, T. B., Shyamsunder, E., and Young, R. D. (1985) *Proc. Natl. Acad. Sci. U.S.A. 82*, 5000−5004.
7. Ansari, A., Berendzen, J., Braunstein, D., Cowen, B. R., Frauenfelder, H., Hong, M. K., Iben, I. E. T., Johnson, J. B., Ormos, P., Sauke, T. B., Scholl, R., Schulte, A., Steinbach, P. J., Vittitow, J., and Young, R. D. (1987) *Biophys. Chem. 26*, 337−355.
8. Frauenfelder, H., Sligar, S. G., and Wolynes, P. G. (1991) *Science 254*, 1598−1603.
9. Griffith, O. W., and Stuehr, D. J. (1995) *Annu. Rev. Physiol. 57*, 707−736.
10. Mayer, B., and Hemmens, B. (1997) *Trends Biochem. Sci. 22*, 477−481.
11. Crane, B. R., Arvai, A. S., Gachhui, R., Wu, C., Ghosh, D. K., Getzoff, E. D., Stuehr, D. J., and Tainer, J. A. (1997) *Science 278*, 425−431.
12. Crane, B. R., Arvai, A. S., Ghosh, D. K., Wu, C., Getzoff, E. D., Stuehr, D. J., and Tainer, J. A. (1998) *Science 279*, 2121−2126.
13. Harteneck, C., Klatt, P., Schmidt, K., and Mayer, B. (1994) *Biochem. J. 304*, 683−686.
14. Livesey, A. K., and Brochon, J.-C. (1987) *Biophys. J. 52*, 693−706.
15. Livesey, A. K., Delaye, M., Licinio, P., and Brochon, J.-C. (1987) *Faraday Discuss. Chem. Soc. 83*, 1−12.
16. Steinbach, P. J., Ansari, A., Berendzen, J., Braunstein, D., Chu, K., Cowen, B. R., Ehrenstein, D., Frauenfelder, H., Bruce Johnson, J., Lamb, D. C., Luck, S., Mourant, J. R., Nienhaus, G. U., Ormos, P., Philipp, R., Xie, A., and Young, R. D. (1991) *Biochemistry 30*, 3988−4001.
17. Steinbach, P. J., Chu, K., Frauenfelder, H., Johnson, J. B., Lamb, D. C., Nienhaus, G. U., Sauke, T. B., and Young, R. D. (1992) *Biophys. J. 61*, 235−245.
18. Johnson, J. B., Lamb, D., Frauenfelder, H., Müller, J., McMahon, B., Nienhaus, G. U., and Young, R. D. (1996) *Biophys. J. 71*, 1563−1573.
19. Lavalette, D., Amand, B., and Pochon, F. (1977) *Proc. Natl. Acad. Sci. U.S.A. 74*, 1407−1411.
20. Matsuoka, A., Stuehr, D. J., Olson, J. S., Clark, P., and Ikeda-Saito, M. (1994) *J. Biol. Chem. 269*, 20335−20339.
21. Scheele, J. S., Kharitonov, V. G., Martasek, P., Roman, L. J., Sharma, V. S., Masters, B. S. S., and Madge, D. (1997) *J. Biol. Chem. 272*, 12523−12528.
22. Wang, J., Stuehr, D. J., and Rousseau, D. L. (1997) *Biochemistry 36*, 4595−4606.
23. Tao, T. (1969) *Biopolymers 8*, 609−632.
24. Klatt, P., Schmidt, K., Lehner, D., Glatter, O., Bächinger, H. P., and Mayer, B. (1995) *EMBO J. 14*, 3687−3695.
25. Abu-Soud, H. M., Wu, C., Ghosh, D. K., and Stuehr, D. J. (1998) *37*, 3777−3786.
26. Sato, H., Nomura, S., Sagami, I., Ito, O., Daff, S., and Shimizu, T. (1998) *FEBS Lett. 430*, 377−380.
27. Tierney, D. L., Martasek, P., Doan, P. E., Masters, B. S. S., and Hoffman, B. M. (1998) *J. Am. Chem. Soc. 120*, 2983−2984.
28. Poulos, T. L., Finzel, B. C., Gunsalus, I. C., Wagner, G. C., and Kraut, J. (1985) *J. Biol. Chem. 260*, 16122−16130.
29. Poulos, T. L., Raman, C. S., and Li, H. (1998) *Structure 6*, 255−258.
30. Alben, J. O., Beece, D., Bowne, S. F., Doster, W., Eiseinstein, L., Frauenfelder, H., Good, D., McDonald, J. D., Marden, M. C., Moh, P. P., Reinisch, L., Reynolds, A., Shyamsunder, E., and Yue, K. T. (1982) *Proc. Natl. Acad. Sci. U.S.A. 79*, 3744−3748.
31. Jung, C., Ristau, O., Schulze, H., and Sligar, S. G. (1996) *Eur. Biochem. J. 235*, 660−669.
32. Schulze, H., Hui Bon Hoa, G., Helms, V., Wade, R. C., and Jung, C. (1996) *Biochemistry 35*, 14127−14137.
33. El-Kasmi, D., Tetreau, C., Lavalette, D., and Momenteau, M. (1995) *J. Am. Chem. Soc. 117*, 6041−6047.

BI9901026